Open Ceramics 16 (2023) 100496

Contents lists available at ScienceDirect

Open Ceramics

journal homepage: www.sciencedirect.com/journal/open-ceramics

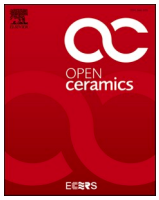

The role of paraffin wax on the properties and printability of ethylene vinyl acetate-based feedstocks for alumina fused filament fabrication

Milan Vukšić [a], Marko Bek [b], Lidija Slemenik Perše [b], Marjeta Maček Kržmanc [c], Andraž Kocjan [a], Aljaž Iveković [a,*]

[a] Department for Nanostructured Materials, Jozef Stefan Institute, Ljubljana, Slovenia
[b] University of Ljubljana, Faculty of Mechanical Engineering, Ljubljana, Slovenia
[c] Advanced Materials Department, Jozef Stefan Institute, Ljubljana, Slovenia

ARTICLE INFO

Handling Editor: Dr P Colombo

ABSTRACT

Fused filament fabrication (FFF) is a versatile and inexpensive additive manufacturing (AM) technique for fabrication of complex shaped ceramic structures. The composition of the binder phase in ceramic-filled feedstock is crucial in determining its rheological behaviour during processing as well as the ability to obtain a defect-free part following debinding and sintering. In this study, the effect of paraffin wax (PW) addition to alumina feedstock with ethylene vinyl acetate (EVA) binder, on feedstock preparation, printability, and debinding has been investigated. The PW incorporation resulted in successful fabrication of a flexible filament with a bending (fracture) strain of 4±1 %. The addition of PW however did not have a significant impact on the debinding of the developed alumina filaments. The printed parts could only be successfully debinded up to 2 mm wall thickness. The subsequent sintering of the debinded parts resulted in a relative density of 98 %.

1. Introduction

The most common form of material extrusion (MEX) additive manufacturing technology is fused filament fabrication (FFF), also referred to as fused deposition modeling (FDM). The method is based on the melting, extrusion, and deposition of thermoplastic filament material, followed by its solidification in a layer-by-layer manner according to a designed deposition trajectory path [1]. FFF offers a possibility for simple, cost-effective fabrication of complex-shaped components [2] by utilizing various polymers or polymer-based composites [3–5]. A variant of the FFF process was also developed for the production of ceramic and metallic components. A thermoplastic polymer which acts as a binder, is highly-filled with ceramic or metallic powder [6]. Shaping of the component follows the conventional FFF approach by utilizing the thermoplastic nature of the powder-binder mixture. Additional steps of binder removal (debinding) and densification (sintering) are required to obtain a pure ceramic (or metal) component [4]. High solid loading levels are required in order to ensure high green densities with minimal shrinkage and porosity after thermal debinding and sintering. The addition of high solids loading of ceramic filler powder, typically in the range from 45 to 65 vol% [7], presents a challenge for the successful fabrication of flexible filaments with suitable rheological characteristics to enable MEX. Alternatively, screw-based material extrusion enables the extrusion of feedstocks in a pellet form, avoiding the stringent requirements for filament materials [8]. Despite the advantages of using the feedstock in a pellet form (shortened process cycle, flexibility in material selection), low print resolution and surface quality limit their application [9].

The properties of the feedstock depend largely on the selection of an appropriate thermoplastic binder system. Good compatibility between the powder and thermoplastic components is a prerequisite for the homogeneous distribution of powder, enabling high solids loading. The binder must also provide sufficient room temperature flexibility combined with relatively low melt viscosity and adequate strength during the initial stage of binder removal [7]. The binder system typically consists of a backbone polymer, which provides the mechanical properties, and various secondary polymers and additives (e.g. plasticizer, surfactant, …) which ensure suitable rheological behaviour and homogeneity of powder-binder mixture.

Initial binder formulations for ceramic FFF introduced in 1990s were based on feedstock formulations developed initially for powder injection moulding (PIM) with polyolefin (e.g. polyethylene, polypropylene) as

* Corresponding author.
E-mail address: aljaz.ivekovic@ijs.si (A. Iveković).

https://doi.org/10.1016/j.oceram.2023.100496
Received 31 August 2023; Received in revised form 12 October 2023; Accepted 18 October 2023
Available online 23 October 2023

Table 1
List of the investigated ceramic feedstocks (CF).

Feedstock	Al_2O_3	EVA	PW	SA	mSA/A	Extruded Filament	FFF
	wt. %				mg/m2		
CF-0	80.7	18.1	0.0	1.2	1.5	✔	✕
CF-20	81.1	14.1	3.8	1.1	1.5	✔	✔
CF-40	81.1	10.3	7.5	1.1	1.5	✔	✔

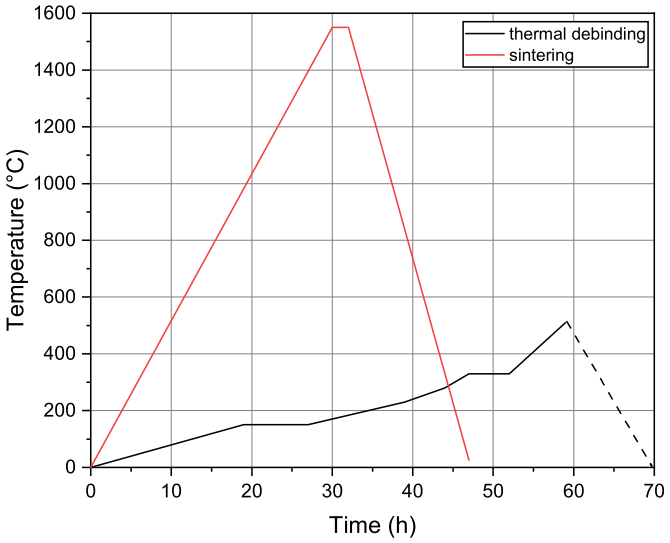

Fig. 1. Thermal (wick) debinding and sintering profile used in this study.

backbone polymer. However, most of this formulations were brittle [10,11], resulting in filaments that could not be winded into spools. While the flexibility of filaments is not essential for material extrusion, it hinders handling and shaping of complex shaped components. If the flexibility of fabricated filaments is too low, the filament cannot be properly spooled resulting in irregular feed rate and formation of defects during printing [7,12,13]. In more recent literature, feedstock formulations are being investigated where elastomeric compounds, most notably ethylene vinyl acetate (EVA), are used to partially [14] or completely replace the backbone polymer [14–17]. Fan et al. [18] noted that sufficient amount of EVA (≥30 %) is necessary to achieve a suitable filament flexibility for FFF. Gorjan et al. [15] investigated the combination of EVA and stearic acid (SA) as a surfactant and plasticizer, to form alumina-filled filaments. SA concentration of 17 wt% was required to ensure good printability, however, high SA concentrations resulted in a more brittle and less flexible filament. Furthermore, in a following study, Conzelmann et al. [19] reported that only thin specimens could be successfully debinded, whereas, thicker specimens resulted in specimen bloating and formation of large voids. The formation of voids was attributed to the decomposition of EVA and formation of acetic acid as reported by Hrdina et al. [20]. Similar observation were also made for FFF of zirconia with binder system consisting of a mixture of two EVA polymers with different vinyl acetate content and stearic acid [21].

EVA was also studied as a minor (backbone) binder in PIM of metals [22] and ceramics [23,24]. The major constituent of the binder was paraffin wax (PW), which is removed either chemically or by low temperature (wick) debinding [23], to form a porous network which enables easier removal of a second (backbone) polymer during thermal debinding [22]. Similar approach was adopted also in this study. In order to facilitate the debinding process while still retaining the benefits of elastomeric nature of EVA, the effect of PW addition was investigated. It was speculated that addition of PW would result in better processability of the formed feedstocks during printing and especially during thermal decomposition of the binder. By removing a sufficient amount of PW during the initial stages of debinding, a more graceful removal of EVA thermal decomposition products was expected.

2. Materials and methods

Thermoplastic feedstock was prepared with 50 vol% of Al_2O_3 powder (A16, Almantis, Germany). The used powder had a monomodal particle size distribution with a median particle size, d_{50} of 0.34 μm with measured specific surface area of 7.91 m^2/g. Specific surface area was measured using a nitrogen-sorption analyser (Nova 2000e, Quantachrome GmbH & Co. KG, USA) and the Brunauer–Emmett–Teller (BET) equation was used for calculations of the specific surface areas.

To evaluate the effect of paraffin wax addition three ceramic feedstock (CF) formulations were prepared (Table 1), where ethylene vinyl acetate (EVA) copolymer binder (Elvax420A, Dupont, USA) was replaced with 0, 20 or 40 % of paraffin wax (VWR, Belgium), noted as CF-0, CF-20 and CF-40, respectively. Stearic acid (Sigma-Aldrich, Germany) was added as a surfactant.

Prior to mixing the powders were dried at 180 °C for 24 h. The preparation of ceramic feedstocks for extrusion (fabrication of filaments) was carried out by manual mixing in a ceramic dish heated to 130 °C. Paraffin wax and stearic acid were put into a heated ceramic dish, followed by addition of EVA pellets. The ceramic powder was gradually added to the binder mixture, followed by intense mixing until all ceramic powder is incorporated into the binder system.

The extrusion was performed at the feed barrel temperature of 60 °C till 130 °C at the orifice with an extrusion speed of 25 rpm (50 mm/s) using a twin-screw extruder (PolyLab, Haake, USA). To ensure good homogenisation the ceramic-based feedstock was passed through the extruder several times, until a constant pressure value at the extrusion nozzle was obtained. The feedstock was extruded through an orifice with diameter of 1.75 mm. To ensure dimensional consistency, the diameter of the produced filament was measured along the length of the filament using a digital calliper. The average obtained diameter was 1.75 ± 0.05 mm.

In order to determine the filament flexibility, filament bending strain was determined by bending in a controlled manner up to a maximum curvature before it fractures [15]. The bend radius (R) is recorded and strain (ε) at the outer edge of the filament with diameter d is calculated according to equation:

$$\varepsilon = \frac{d}{2R} \qquad \text{Equation 1}$$

Rheological measurements were carried out on mixed feedstocks and extruded filaments (CF-0, CF-20, CF-40) using rotational rheometer (Physica MCR301, Anton Paar, Austria) with a 25 mm diameter parallel-plate measuring setup with a fixed gap of 1 mm. Shear viscosity measurements were performed at a constant temperature of 150 °C in the shear rate range from 0.01 to 200 s^{-1}. Small amplitude oscillatory shear (SAOS) measurements were performed to evaluate the viscoelastic properties of the ceramic feedstocks. All measurements were conducted in a linear viscoelastic regime. The shear elastic modulus, G' and the shear loss modulus, G'' were evaluated as a function of temperature at constant frequencies of 0.1 Hz, 1 Hz and 10 Hz. Stress relaxation experiments were carried out at constant strain of 0.1 % at temperatures indicated in the Results and Discussion section.

Thermal analysis measurements were performed on a Jupiter 449 simultaneous thermal analysis (STA) instrument (Netzsch, Selb, Germany) coupled with a 403C Aëoloss mass spectrometer (Netzsch, Selb, Germany). The measurements were made with a heating rate of 10 °C/min in an argon/oxygen (80/20) atmosphere using differential thermal analysis (DTA) sample holder and alumina crucibles.

Rectangular bars of dimensions of 50 mm x 5 mm x 5 mm were printed on a MakerBot Replicator 2X (MakerBot, USA) using a 0.8 mm nozzle. Slicing and adjustment of printing parameters was performed using Simplify3D software (Simplify 3D, USA), where layer height was

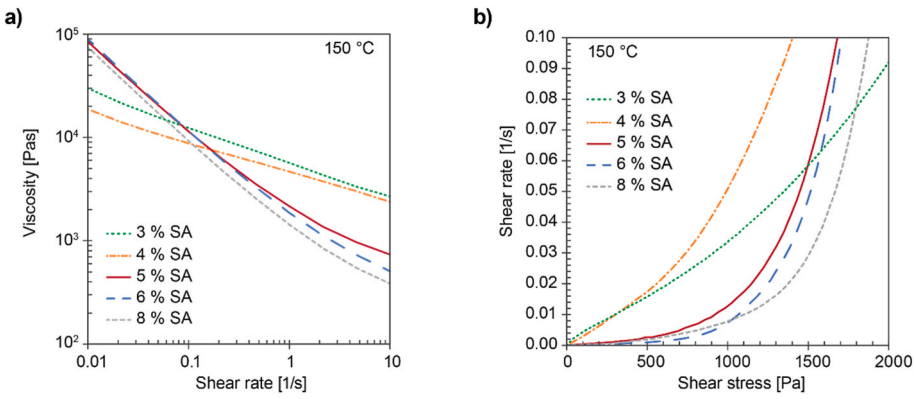

Fig. 2. Shear viscosity a) and yield stress measurements b) as a function of % of stearic acid addition measured at 150 °C for CF-20.

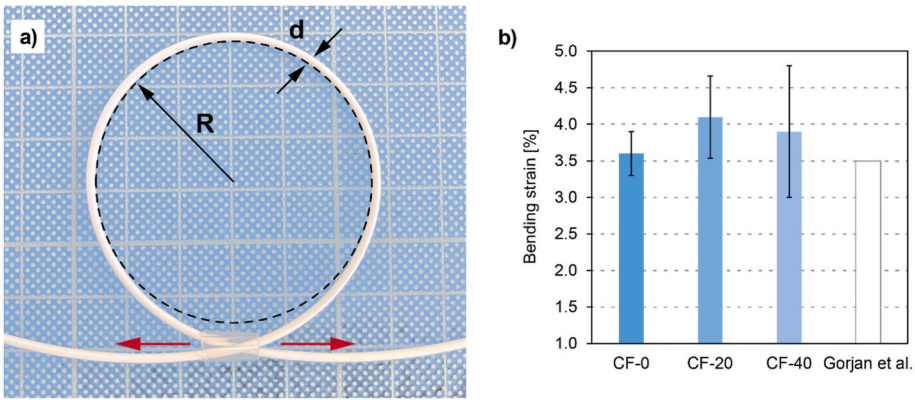

Fig. 3. *a) Determination of filament bending strain and b) comparison of bending strain values for CF-0, CF-20 and CF-40 compared to literature values reported by Gorjan* et al. [15] *for Al_2O_3 filaments with EVA binder and 17 wt% SA.*

kept constant at 0.25 mm, while nozzle temperature and printing speed were varied in order to investigate printability of the developed alumina filament. Disc shaped objects with fixed diameter of 20 mm and thickness in range from 1 mm to 4 mm were 3D printed according to previously determined favourable printing settings in order to investigate debinding behaviour of the green parts. Temperature of the build platform was kept constant at 30 °C in all printing sessions.

Debinding of the green parts was conducted by means of thermal wick debinding where green parts were embedded in a wicking powder bed (Nabalox® NO 201, Nabaltec, Germany) followed by heating in air in a muffle furnace (Nabertherm, Germany) up to 500 °C. Details on the debinding process are presented in Fig. 1. Sintering was performed up to 1550 °C for 2 h in air using the same type of muffle furnace.

The microstructural analysis of the as-printed surface and fractured cross-sections, was done using optical stereo microscope (Discovery V8, Carl Zeiss AG, Germany) and field emission scanning electron microscope (JEOL JSM-7600F, JEOL Ltd., Japan).

3. Results and Discussion

3.1. Feedstock characterisation/filament

Rheology of the feedstock material is crucial for the optimal performance during printing. However, due to the nature of the FFF which utilizes thermoplastic behaviour in order to melt and extrude the feedstock which upon solidification retains its shape, not only the behaviour of molten feedstock, but also room temperature properties must be considered. A suitable feedstock material should provide an appropriate balance between the physical properties in the solid state, and the rheological properties in the molten state.

3.1.1. Stearic acid concentration

In order to assure optimal powder dispersion and processability, the amount of stearic acid was optimized. Measurements of shear viscosity and yield stress were performed on feedstock formulations containing 20 wt% of paraffin wax in the binder composition (CF-20) and varying the amount of stearic acid (SA) from 1 wt% to 10 wt% of binder formulation. As is seen in Fig. 2a, all samples exhibited shear thinning behaviour, however there was a distinct shift in the behaviour between 4 wt% and 5 wt% SA addition. Similar observation was seen in the measurements of shear rate as a function of applied shear stress (Fig. 2b). Yield stress behaviour was only observed for the suspensions containing >5 wt% SA. As was noted by Gorjan et al. [16], yield stress behaviour is essential to ensure the stability of the formed part during the debinding step.

The theoretical value of 2.27 mg/m^2 was reported to obtain a fully saturated monolayer of SA per surface area of ceramic powder [15]. The noticed shift of the curve representing 5 wt% addition of SA corresponds to 1.5 mg/m^2 by considering the BET measured surface area of 7.91 m^2/g for the used A16 powder. The calculated amount of SA is smaller compared to the theoretical one due to particle agglomeration which can result in decrease of the available surface for surfactant adsorption [15]. Considering the measured median particle size (d_{50}=0.34 μm), an idealised specific surface area (BET_{50}) available can be estimated according to the equation:

$$BET_{50} = \frac{6}{d_{50} \bullet \rho} \qquad \text{Equation 2}$$

where ρ is the density of ceramic powder. The BET_{50} calculated value of 4.43 m^2/g is significantly lower than the one determined by BET (7.91 m^2/g), which examines also the interagglomerate porosity. Assessing

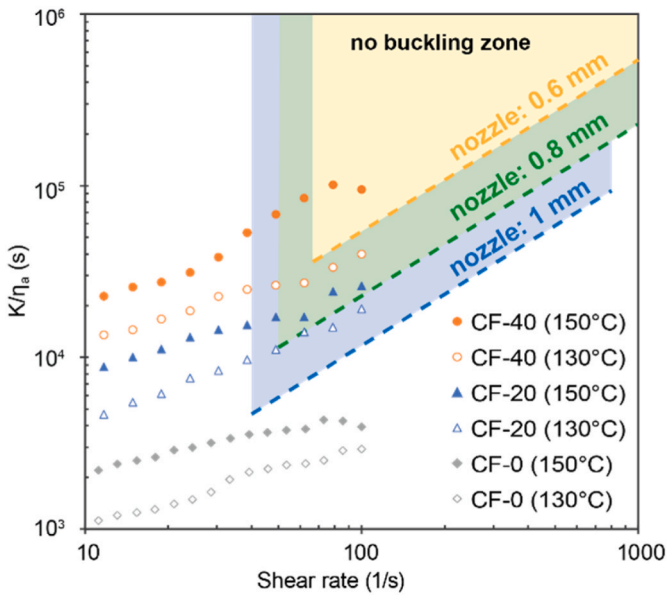

Fig. 4. Assessment of filament buckling conditions based on K/ηa ratio. The coloured areas represent the range where no buckling is expected for nozzle diameters 0.6 mm, 0.8 mm (used in this study) and 1 mm within the apparent shear range determined for printing velocity between 5 and 100 mm/s.

the calculated value, the surface adsorption of SA with 5 wt% addition is 2.7 mg/m^2, which is slightly above the theoretical prediction of 2.27 mg/m^2, and can therefore be used to explain the shift in rheological behaviour of feedstocks with SA concentration >5 wt%. Unadsorbed SA onto the ceramic particle surface can be integrated into the binder matrix, reducing the overall viscosity of the feedstock [25,26] and providing yield stress behaviour through polymeric chain entanglement. To ensure optimal feedstock behaviour (good dispersion of ceramic powder, yield stress behaviour), all further feedstock formulations were prepared with 6 wt% SA addition.

3.1.2. *Filament flexibility*

Initial handling and winding of the produced filaments are governed by their flexibility. Determination of filament bending strain (Fig. 3) was proposed as a comparative measure of filament flexibility in FFF [15]. Filaments from all investigated feedstocks had a comparable bending (fracture) strain of 3.6 ±0.3 %, 4.1±0.6 % and 3.9±0.9 % for feedstocks CF-0, CF-20 and CF-40, respectively. The values are comparable to the ones reported by Gorjan et al. [15] for alumina filaments with EVA-based binder and SA addition above the saturation threshold. The authors concluded that higher SA concentration (>17 wt%) would result in a brittle filament that could not be processed. In the case of PW, no deterioration was observed for higher PW content. All filaments could be processed successfully, nevertheless, careful handling was needed in order to prevent breaking of the filaments.

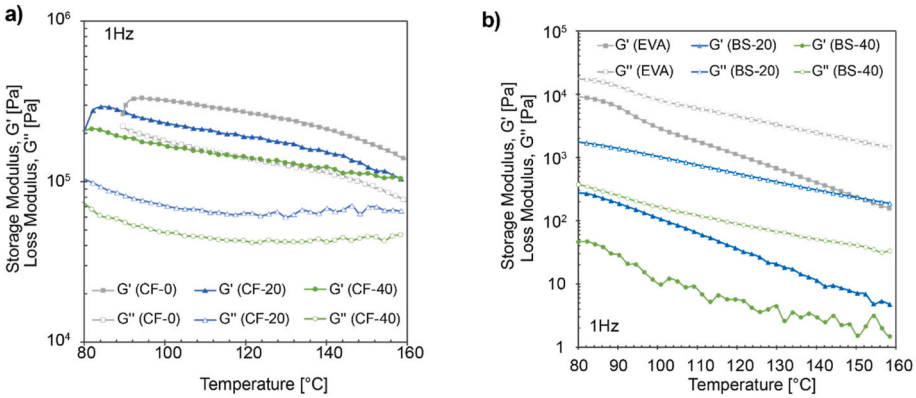

Fig. 5. Storage (G′) and loss modulus (G″) as a function of temperature at a constant frequency of 1 Hz in LVER for a) ceramic feedstocks CF-0, CF-20 and CF-40, b) EVA and binder systems.

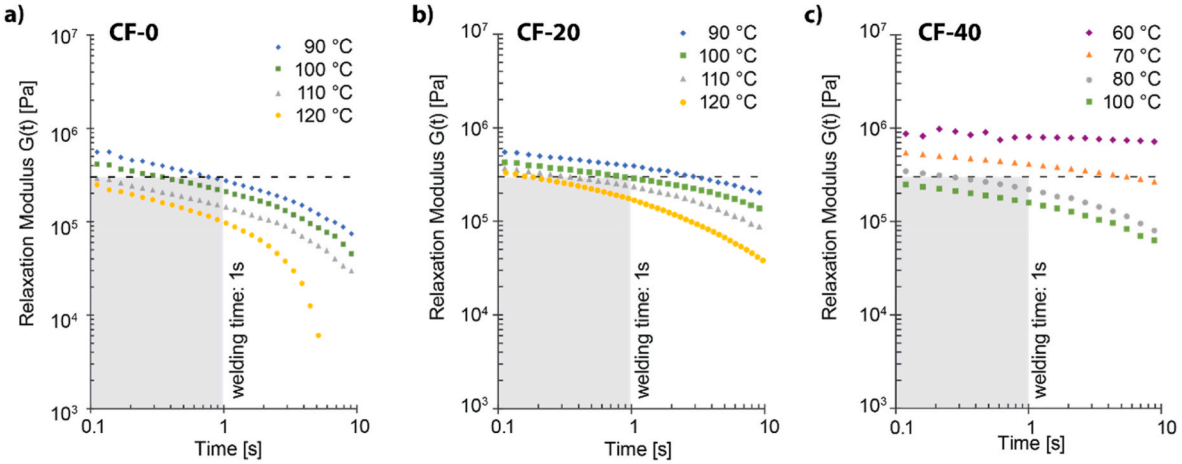

Fig. 6. Stress relaxation experiments performed at different temperatures for a) CF-0, b) CF-20 and c) CF-40 filament feedstock. The dashed line represents the Dahlquist criterion value of 3x10^5 Pa.

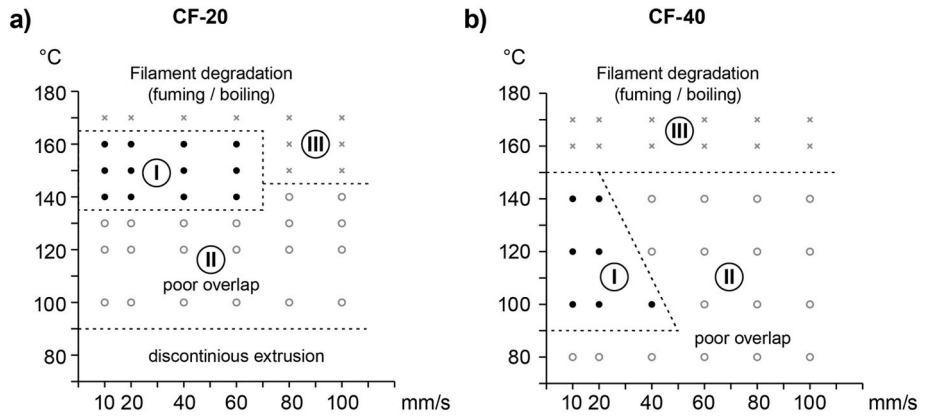

Fig. 7. FFF printability experiments for a) feedstock CF-20 and b) CF-40. All experiments were performed with 0.8 mm nozzle and constant layer height of 0.25 mm.

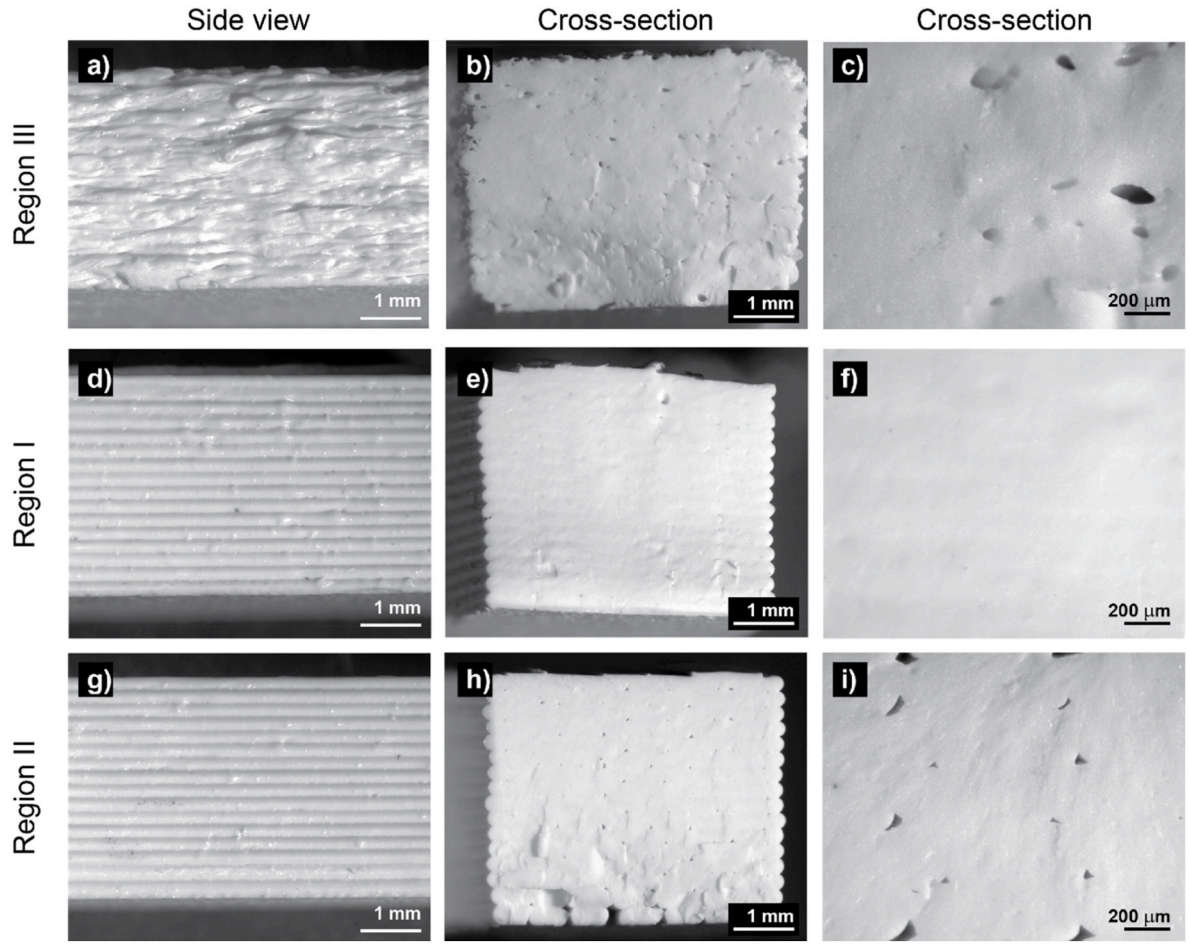

Fig. 8. Optical micrographs of representative samples printed from filament from feedstock CF-20, for individual printability regions, I (d–f), II (g–i) and III (a–c).

3.1.3. Filament stiffness (buckling)

In order to avoid filament buckling during extrusion, the pressure required to produce the flow should be smaller than the critical stress for buckling. Venkataraman [27] developed a methodology for characterisation of compressive mechanical properties of ceramic particle filled thermoplastic filaments, based on the ratio between compression modulus K and apparent viscosity (η_a). According to equation:

$$\frac{K}{\eta_a} > \frac{8Ql\left(L/R\right)^2}{\pi^3 r^4} \qquad \text{Equation 3}$$

where Q is volumetric flow rate, R is the filament radius, L is the length between the extrusion mechanism and the printing head, and l and r are length and radius of the nozzle respectively. Assuming the mass conservation, the volumetric flow rate can be calculated from printing velocity (v_p) and diameter of the printing nozzle:

$$Q = \pi R^2 v_p \qquad \text{Equation 4}$$

According to Equation (3), for a given printer configuration geometry and flow rate, filaments with a value of K/η_a higher than a critical value (represented by dashed lines in Fig. 4), are assumed to be suitable for FFF avoiding buckling.

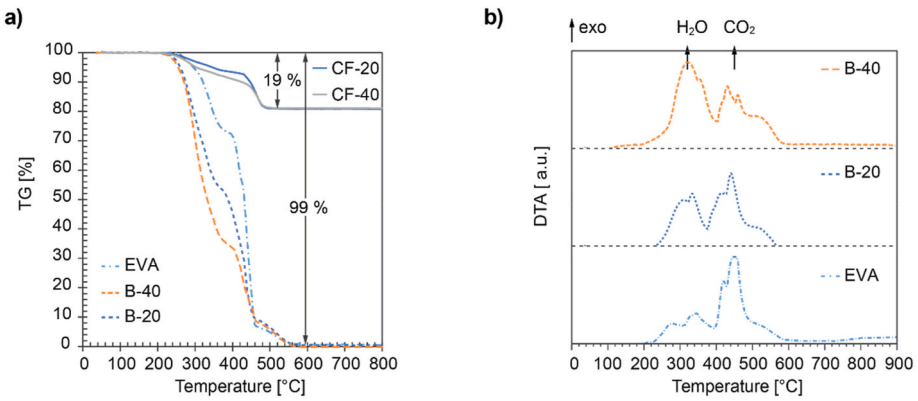

Fig. 9. a) TG and b) DTA analysis of feedstock (CF-20 and CF-40) and binder formulations (EVA, B-20, B-40) at 10 K/min.

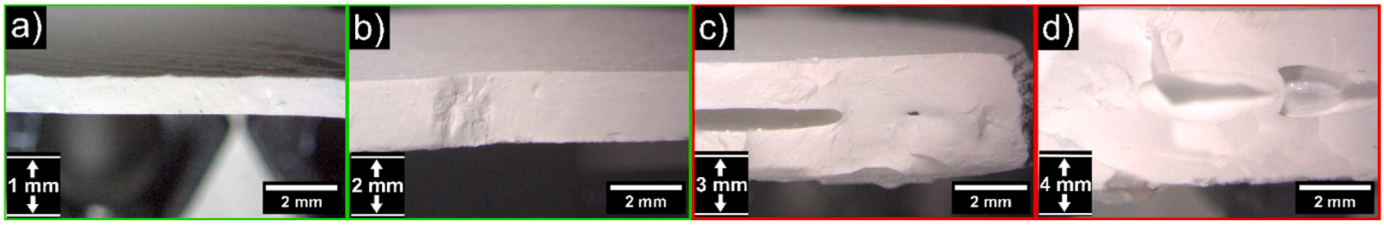

Fig. 10. Samples with various thickness fabricated from CF-40, after thermal debinding in the powder bed: a) 1 mm, b) 2 mm, c) 3 mm, and d) 4 mm.

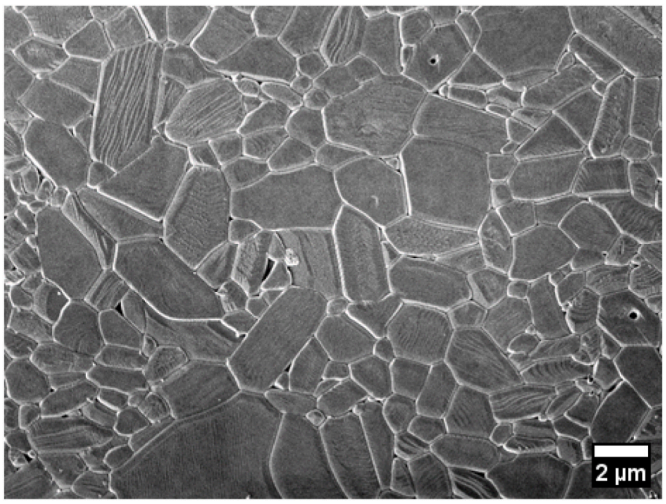

Fig. 11. Polished and thermally etched microstructure of sample form feedstock CF-40 after sintering.

As expected the addition PW decreases the viscosity of feedstocks as PW acts as a plasticizer. Due to slippage of the feedstock during shear viscosity measurements, viscosity measurements could only be performed at low shear rates (<100 s^{-1}). Fig. 4 depicts the K/η_a ratio, with K measured at room temperature and viscosity at 130 °C and 150 °C. K/η_a ratio was calculated for nozzle diameters of 0.6 mm, 0.8 mm (used experimentally in this study) and 1 mm with a fixed length of 12 mm between rollers and the top of the heated nozzle (L) and nozzle length (l) of 0.5 mm.

Dashed lines represent the critical values of K/η_a ratio, below which filament buckling is expected in the range of apparent shear rate ($\dot{\gamma}$) calculated according to Equation (5) [28]:

$$\dot{\gamma} = \frac{4 \bullet Q}{\pi \bullet r^3} = \frac{4 \bullet v}{r} \qquad \text{Equation 5}$$

for minimum and maximum print velocity (v) of 5 mm/s and 100 mm/s, respectively. From Fig. 4 it is evident that by decreasing the nozzle size, the probability of filament buckling is increased. Probability of buckling is also increased at higher shear rates (higher printing speeds) and lower printing temperatures.

In the case of CF-0 feedstock, buckling is expected for all nozzle sizes in the range of investigated print velocities. On the other hand, feedstocks CF-20 and CF-40 could be processed without buckling, where

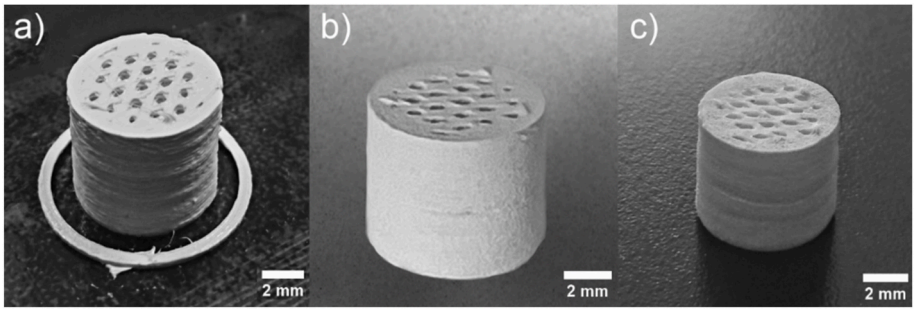

Fig. 12. Scaffold structure a) as printed from CF-40, b) after thermal debinding in powder bed, and c) after sintering at 1550 °C.

feedstock CF-20 would require higher nozzle diameters (>0.8 mm) and processing temperatures (>150 °C) in order to avoid printing failure. Due to the small difference in measured compression modulus (*K*) between feedstocks CF-20 (2.26 MPa) and CF-40 (2.18 MPa), the feedstock viscosity appears to be the governing parameter in determining the buckling probability.

Based on this analysis, a decreased viscosity at higher paraffin wax concentrations (and/or higher temperatures) has a beneficial effect in preventing filament buckling and facilitates extrusion with smaller nozzle sizes.

3.1.4. Filament flow behaviour

Next to filament buckling, nozzle clogging is often the reason for print failure during FFF. To evaluate the feedstock flow behaviour, viscoelastic properties of molten feedstock should be considered. Ideally, the transition from solid to liquid behaviour ($G'=G''$), which denotes the temperature above which no clogging is expected.

Temperature sweep experiments at constant frequency, conducted in a linear viscoelastic regime offer an insight into interparticle and flow behaviour of the feedstock material. Fig. 5 shows the storage (G') and loss moduli (G'') results as a function of temperature of investigated feedstock materials (CF-0, CF-20 and CF-40), as well as bare binder systems with 0, 20 and 40 wt% paraffin wax addition. Ceramic feedstocks exhibited predominantly solid behaviour, with $G'>G''$ over the entire investigated temperature range (80–160 °C). The CF-0 feedstock could only be evaluated above 90 °C. The solid behaviour of the feedstock materials can be attributed to the high concentration of the ceramic powders, which contribute to G', and thus prevents the observation of $G'=G''$ transition.

To further elucidate the viscoelastic behaviour, only binder compositions without added ceramic powder were also evaluated (Fig. 5b). Unlike the behaviour of ceramic feedstocks, all binder compositions exhibit liquid behaviour ($G''>G'$) over the evaluated temperature range. PW acts as a plasticizer in both binder system as well as to the feedstock, which is reflected in Fig. 5a), b). The easier movement of polymeric molecules is enabled by increasing the content of low molecular weight PW what is noticeable from decrease of both G' and G'' (Fig. 5a).

3.1.5. Welding between layers

Extrusion of the feedstock filaments is only the first step to a successful printing of ceramic green bodies. The adhesion of the feedstock material to the substrate as well as welding between consecutively deposited layers is crucial for the fabrication of sound parts. Adhesion between layers is favoured for materials with a predominantly viscous behaviour at welding temperature ($G''>G'$), which does not apply in our system as discussed in the previous section. Alternatively, a methodology based on Dahlquist criterion, initially developed for adhesives, was proposed as a representative parameter for successful interlayer welding [29]. According to the Dahlquist criterion, instantaneous layer adhesion is obtained below a critical elastic modulus value of 3 x 10^5 Pa (which corresponds to the compliance value of 10^{-5} Pa^{-1}), regardless of the G'' over G' state.

The adhesion temperature depends on the printing parameters (e.g. nozzle temperature, nozzle dimensions, extrusion velocity, …), convective cooling from the air moving in the build environment, material properties of the used feedstock (glass transition temperature, thermal conductivity) and cooling time. Seppala et al. [30] determined that polymer based feedstocks remain above glass transition temperature required for successful bonding, for the cooling time of approximately 1 s. As thermal conductivity of Al_2O_3 is two orders of magnitude higher than that of polymers, the time required to dissipate the heat and solidify the material is expected to be significantly lower. However, Bellini [31] demonstrated, that the greater the thermal conductivity of the melt the slower the material will cool on leaving the extrusion nozzle. Determination of the actual welding temperature and time was not conducted within the scope of this work; therefore, solidification time of 1 s was adopted also in our study to facilitate the comparison between different feedstock formulations.

Using aforementioned criteria, a minimum temperature for interlayer adhesion can be determined by performing stress relaxation experiments. As mentioned previously, feedstock CF-0 could only be evaluated at temperatures >90 °C, where it already satisfied the Dahlquist criterion assuming the welding time of 1 s (Fig. 6a). By increasing temperature and resulting higher molecular mobility, even lower relaxation time was needed in order to satisfy the condition for instantaneous adhesion. With the addition of PW (CF-20), longer relaxation times were required at comparable temperatures in order for $G(t)$ to fall below the threshold value. On the other hand, in the case of feedstock CF-40, further PW addition resulted in significantly reduced values of the initial stress and consequently the temperature required for interlayer adhesion. Considering the solidification time of 1 s, interlayer welding can be expected at temperatures >100 °C and >80 °C, for feedstocks CF-20 and CF-40, respectively (Fig. 6b–c). Higher mobility of PW chains decreases the initial stress and results in lower values of relaxation modulus.

3.2. Printability evaluation

Printability of each feedstock was evaluated predominantly in terms of printing temperature and printing speed. Feedstock without the addition of PW (CF-0) could not be printed due to discontinuous extrusion and deformation of the filament in the printhead. Failure to properly extrude the CF-0 feedstock is in line with the predictions in section 3.1.3. Similar observation was also made by Gorjan et al. [15] who noted that insufficient amount of stearic acid addition resulted in feedstocks that were not printable. The addition of SA above the apparent saturation of the powder surface, acted as a plasticizer in a similar manner as PW in our study and optimal results were obtained with 17 wt% of SA, however, higher concentrations were not evaluated.

For printability of feedstocks CF-20 and CF-40, three distinct regions of temperature-speed combinations were observed (Fig. 7): I – sound prints without any observable defects, II – sound prints with small defects indicating poor overlap of neighbouring lines, III – printed parts with poor surface quality and spherical defects in the bulk.

In the case of CF-20, optimal printing results were achieved in the temperature range between 140 and 160 °C and printing speeds below 60 mm/s (region I, Fig. 7a). At low printing temperature, samples could be realized, however, observation of the as-printed fracture surface revealed residual porosity due to poor overlap of the extruded material (region II), which was more pronounced at higher printing speed. The appearance of smaller defects (Fig. 8i) at low printing speeds (10–60 mm/s) could most likely be eliminated by increasing the extrusion multiplier in the slicing software, however that was not investigated as a part of this study. At temperatures above 170 °C, the samples were characterized by a poor surface finish and the presence of voids within the cross-section (region III). Unlike defects observed at low temperature, the pores appeared more spherical (Fig. 8c), which might indicate the onset of binder degradation. Paraffin wax thermally decomposes at 210 °C, however, the decomposition of stearic acid occurs already at lower temperature of 160 °C [32], which might result in void formation. At temperatures above 180 °C the filament degradation with boiling and fuming at the nozzle was clearly observed and prevented successful fabrication.

As mentioned, similar distinct regions were also observed when printing with CF-40 filament, however, the optimal printability window (region I) was decreased and shifted toward lower temperatures between 100 and 140 °C and speeds below 40 mm/s (Fig. 7b). Shift toward lower temperatures can be explained by the lower feedstock viscosity in comparison to CF-20.

3.3. Debinding and sintering

3.3.1. Thermal analysis

Thermal gravimetric analysis was performed on both binder formulations as well as ceramic feedstock materials. For the ceramic feedstocks, approximately 19 wt% mass loss is observed up to 500 °C (Fig. 9a, curves for CF-20 and CF-40). Mass loss is in a good agreement with the total weight of the binder phase, 18.9 wt%, for both investigated compositions. By examining the mass loss of the EVA polymer and the individual binder compositions, we observe that the decomposition of EVA is initiated at 230 °C with complete decomposition achieved at 550 °C (Fig. 9a). According to literature [33], EVA decomposes by a two-step mechanism to acetic acid (300–350 °C) in the first followed by buthene and ethylene in the second (~430 °C). The addition of paraffin wax (samples B-20 and B-40) promoted the decomposition of the binder phase with increased weight loss between 230 °C and 400 °C (Fig. 9b). Above 450 °C the decomposition follows the mass curve of EVA polymer. Addition of paraffin wax to EVA results in a more uniform, gradual decomposition of the binder.

According to the mass spectroscopy, CO_2 and H_2O are the main products of binder decomposition since in the presence of oxygen all intermediate decomposition products are decomposed further to CO_2 and H_2O.

3.3.2. Thermal debinding

Initially experiments with thermal debinding resulted in sample swelling and formation of large voids within the sample. Similar observations for EVA based binder systems were already reported in the literature [20,34,35]. The authors concluded that only thin samples could be successfully debinded due to the limited diffusion of acetic acid during EVA decomposition [19]. Successful debinding of samples with increased wall thickness is hindered by remained residual binder which ultimately results in swelling of the sample and formation of voids within sample structure [36].

In order to successfully remove all binder components and determine maximum wall thickness of the printed parts, thermal debinding of samples with increasing thickness was performed in the powder bed (wick debinding) [37]. Partial wick debinding was performed in multiple stages as illustrated in (Fig. 1). Initial hold temperature of 150 °C, below thermal degradation of binder components (Fig. 9), was used to allow the removal of paraffin wax through capillary action and achieve interconnected pore channels facilitating the escape of gaseous species, which have been generated by decomposition of EVA backbone polymer at higher temperatures. Dwell time of 8 h was necessary to achieve 3 wt % and 5 wt% losses of total mass attributed to the PW degradation in CF-20 and CF-40, respectively. The additional dwell time of 5 h at 320 °C was applied due to exothermic reactions during EVA decomposition which can result in an overshooting of the heating rate and lead to high formation of gases resulting in defects inside the ceramic parts [21]. Following the debinding cycle, the samples were fractured and investigated for internal defects. No deformation was observed in samples with up to 2 mm thickness (Fig. 10a–b). At higher sample thickness void formation in the central part of the samples was observed (Fig. 10c–d), which resulted in swelling of the samples.

3.3.3. Sintering

Following the complete removal of the organic binder phases, the samples were sintered in order to achieve a dense ceramic component. Conventional sintering in air was performed, with holding time of 2 h at maximum temperature of 1550 °C (Fig. 1). The resulting samples were densified up to 98 % TD regardless of the binder composition (Fig. 11). Dimensional shrinkages in X, Y and Z directions were determined as follows: X, Y = 16.75±1 %; Z = 22.5±1 %.

The optimized printing and debinding procedures were applied to fabricate scaffold structure. More precisely, a cylindric shape with the radius of circular base of 7.5 mm and the height of 12 mm. The designed porosity of the scaffold structure was controlled by setting the 50 % infill which resulted in maximal wall thickness of 2 mm to enable defect free debinding of the printed scaffold (Fig. 12).

Although the structures in Fig. 12 demonstrate the ability to utilize such feedstocks to fabricate simple 3-dimensional objects, fabrication of smaller complex shaped parts remains challenging. High viscosity of feedstocks containing large amount of ceramic powders favours extrusion through larger nozzles, thus limiting the lateral resolution of the printed objects. Furthermore, the ability to successfully print complex shapes is only the initial step in obtaining sound ceramic components. The debinding and sintering steps are often the limiting processes and require careful selection of powder - binder system combination. The binder system based on EVA and PW allows for successful debinding of Al_2O_3 components with up to 2 mm wall thickness. In order to fabricate thicker components EVA backbone polymer would have to be partially or completely replaced to allow complete decomposition and removal of binder system without formation of defects.

4. Conclusion

Alumina ceramic filled thermoplastic filaments with high solids loading (50 vol%) of Al_2O_3 powder were successfully produced using EVA-based binder system, with stearic acid as a surfactant (1.5 mg/m^2) and various amounts of paraffin wax (0, 20 or 40 wt %) as a plasticizer. All feedstocks were successfully mixed and extruded into filaments of acceptable dimensions (1.75 ± 0.05 mm) and sufficient flexibility, however only filaments with 20 and 40 wt% of PW addition could be processed with FFF.

The addition of paraffin wax to EVA-based binder facilitates the feedstock preparation, printability and to a certain extent also debinding. The addition of paraffin wax didn't significantly affect the filament's flexibility, however, at higher concentrations (40 wt %) considerable impact on stability regarding lower printing temperatures has been observed. Rheological characterisation of a ceramic filled feedstock material was successfully used as an indicator of feedstock behaviour and processability. However, high concentration of ceramic particles makes it difficult to directly correlate the predicted results (e.g. flow behaviour, interlayer adhesion) to experimental observations.

Printed feedstock material could be successfully thermally debinded and sintered to form ceramic material with up to 98 %TD. Although the addition of paraffin wax enables a more controlled debinding, the formation of acetic acid and formation of voids limits the successful debinding of thicker parts (>2 mm).

Declaration of competing interest

The authors declare that they have no known competing financial interests or personal relationships that could have appeared to influence the work reported in this paper.

Acknowledgement

This work was supported by the Slovenian Research Agency funding through research programs Ceramics and complementary materials for advanced engineering and biomedical applications (P2–0087) and Sustainable Polymer Materials and Technologies (P2-0264).

References

[1] Z. Chen, Z. Li, J. Li, C. Liu, C. Lao, Y. Fu, C. Liu, Y. Li, P. Wang, Y. He, 3D printing of ceramics: a review, J. Eur. Ceram. Soc. 39 (2019) 661–687, https://doi.org/10.1016/j.jeurceramsoc.2018.11.013.

[2] M. Harris, J. Potgieter, R. Archer, K.M. Arif, Effect of material and process specific factors on the strength of printed parts in fused filament fabrication: a review of recent developments, Materials 12 (2019), https://doi.org/10.3390/ma12101664.

[3] K. Balamurugan, M. Venkata Pavan, S.K. Ahamad Ali, G. Kalusuraman, Compression and flexural study on PLA-Cu composite filament using FDM, Mater. Today Proc. 44 (2021) 1687–1691, https://doi.org/10.1016/j.matpr.2020.11.858.

[4] M. Orlovská, Z. Chlup, Ľ. Bača, M. Janek, M. Kitzmantel, Fracture and mechanical properties of lightweight alumina ceramics prepared by fused filament fabrication, J. Eur. Ceram. Soc. 40 (2020) 4837–4843, https://doi.org/10.1016/j.jeurceramsoc.2020.02.026.
[5] K. Kim, J. Park, J. Suh, M. Kim, Y. Jeong, I. Park, 3D printing of multiaxial force sensors using carbon nanotube (CNT)/thermoplastic polyurethane (TPU) filaments, Sensors Actuators A Phys 263 (2017) 493–500, https://doi.org/10.1016/j.sna.2017.07.020.
[6] P. B.A, L. N, A. Buradi, S. N, P. B L, V. R, A comprehensive review of emerging additive manufacturing (3D printing technology): methods, materials, applications, challenges, trends and future potential, Mater. Today Proc. 52 (2022) 1309–1313, https://doi.org/10.1016/j.matpr.2021.11.059.
[7] M.R. Ismael, F. Clemens, T. Graule, M.J. Hoffmann, Effects of different thermoplastic binders on the processability of feedstocks for ceramic co-extrusion process, Ceram. Int. 37 (2011) 3173–3182, https://doi.org/10.1016/j.ceramint.2011.05.084.
[8] Z. Zhou, I. Salaoru, P. Morris, G.J. Gibbons, Additive manufacturing of heat-sensitive polymer melt using a pellet-fed material extrusion, Addit. Manuf. 24 (2018) 552–559, https://doi.org/10.1016/j.addma.2018.10.040.
[9] S.C. Altıparmak, V.A. Yardley, Z. Shi, J. Lin, Extrusion-based additive manufacturing technologies: state of the art and future perspectives, J. Manuf. Process. 83 (2022) 607–636, https://doi.org/10.1016/j.jmapro.2022.09.032.
[10] D. Nötzel, T. Hanemann, New feedstock system for fused filament fabrication of sintered alumina parts, Materials 13 (2020), https://doi.org/10.3390/ma13194461. Art.-Nr.
[11] D. Nötzel, R. Eickhoff, T. Hanemann, Fused filament fabrication of small ceramic components, Materials 11 (2018), https://doi.org/10.3390/ma11081463.
[12] M.K. Agarwala, A. Bandyopadhyay, R. van Weeren, A. Safari, S.C. Danforth, N. A. Langrana, V.R. Jamalabad, P.J. Whalen, FDC, Rapid Fabrication of Structural Components, 1996, p. 75. https://www.osti.gov/biblio/409688.
[13] S. Onagoruwa, S. Bose, A. Bandyopadhyay, Fused Deposition of Ceramics (FDC) and Composites, Proceeding SFF Symp. Held., 2001.
[14] A. Hadian, M. Fricke, A. Liersch, F. Clemens, Material extrusion additive manufacturing of zirconia parts using powder injection molding feedstock compositions, Addit. Manuf. 57 (2022), 102966, https://doi.org/10.1016/j.addma.2022.102966.
[15] L. Gorjan, C. Galusca, M. Sami, T. Sebastian, F. Clemens, Effect of stearic acid on rheological properties and printability of ethylene vinyl acetate based feedstocks for fused filament fabrication of alumina, Addit. Manuf. 36 (2020), 101391, https://doi.org/10.1016/j.addma.2020.101391.
[16] L. Gorjan, L. Reiff, A. Liersch, F. Clemens, Ethylene vinyl acetate as a binder for additive manufacturing of tricalcium phosphate bio-ceramics, Ceram. Int. 44 (2018) 15817–15823, https://doi.org/10.1016/j.ceramint.2018.05.260.
[17] F. Sarraf, A. Hadian, S. V Churakov, F. Clemens, EVA-PVA binder system for polymer derived mullite made by material extrusion based additive manufacturing, J. Eur. Ceram. Soc. 43 (2023) 530–541, https://doi.org/10.1016/j.jeurceramsoc.2022.10.009.
[18] N.C. Fan, W.C.J. Wei, B.H. Liu, A.B. Wang, R.C. Luo, Ceramic feedstocks for additive manufacturing, in: 2016 IEEE Int. Conf. Ind. Technol., 2016, pp. 1147–1151, https://doi.org/10.1109/ICIT.2016.7474917.
[19] N.A. Conzelmann, L. Gorjan, F. Sarraf, L.D. Poulikakos, M.N. Partl, C.R. Müller, F. J. Clemens, Manufacturing complex AlO ceramic structures using consumer-grade fused deposition modelling printers, Rapid Prototyp. J. 26 (2020) 1035–1048, https://doi.org/10.1108/RPJ-05-2019-0133.
[20] K.E. Hrdina, J.W. Halloran, M. Kaviany, A. Oliveira, Defect formation during binder removal in ethylene vinyl acetate filled system, J. Mater. Sci. 34 (1999) 3281–3290, https://doi.org/10.1023/A:1004698310477.
[21] A. Hadian, L. Koch, P. Koberg, F. Sarraf, A. Liersch, T. Sebastian, F. Clemens, Material extrusion based additive manufacturing of large zirconia structures using filaments with ethylene vinyl acetate based binder composition, Addit. Manuf. 47 (2021), 102227, https://doi.org/10.1016/j.addma.2021.102227.
[22] M.T. Zaky, F.S. Soliman, A.S. Farag, Influence of paraffin wax characteristics on the formulation of wax-based binders and their debinding from green molded parts using two comparative techniques, J. Mater. Process. Technol. 209 (2009) 5981–5989, https://doi.org/10.1016/j.jmatprotec.2009.07.018.
[23] J. Zorzi, C. Perottoni, J. Jornada, Wax-based binder for low-pressure injection molding and the robust production of ceramic parts, Ind. Ceram. 23 (2003).
[24] T. Standring, S. Blackburn, P. Wilson, Investigation into paraffin wax and ethylene vinyl acetate blends for use as a carrier vehicle in ceramic injection molding, Polym. Plast. Technol. Eng. 55 (2016) 802–817, https://doi.org/10.1080/03602559.2015.1132434.
[25] T.-Y. Chan, S.-T. Lin, Effects of stearic acid on the injection molding of alumina, J. Am. Ceram. Soc. 78 (1995) 2746–2752, https://doi.org/10.1111/j.1151-2916.1995.tb08050.x.
[26] C. Kukla, S. Cano Cano, C. Holzer, J. Gonzalez-Gutierrez, Influence of stearic acid in feedstocks for FFF and PIM, in: Euro PM2019, Maastricht, 2019. https://www.europm2019.com/.
[27] N. Venkataraman, S. Rangarajan, M.J. Matthewson, B. Harper, A. Safari, S. C. Danforth, G. Wu, N. Langrana, S. Guceri, A. Yardimci, Feedstock material property – process relationships in fused deposition of ceramics (FDC), Rapid Prototyp. J. 6 (2000) 244–253, https://doi.org/10.1108/13552540010373344.
[28] C. Brauner, M. Küng, D. Arslan, C. Maurer, Fused filament fabrication based on polyhydroxy ether (phenoxy) polymers and related properties, Polymers 13 (2021), https://doi.org/10.3390/polym13101549.
[29] I. Calafel, R.H. Aguirresarobe, M.I. Peñas, A. Santamaria, M. Tierno, J.I. Conde, B. Pascual, Searching for rheological conditions for FFF 3D printing with PVC based flexible compounds, Materials 13 (2020), https://doi.org/10.3390/ma13010178.
[30] J.E. Seppala, K.D. Migler, Infrared thermography of welding zones produced by polymer extrusion additive manufacturing, Addit. Manuf. 12 (2016) 71–76, https://doi.org/10.1016/j.addma.2016.06.007.
[31] A. Bellini, Fused Deposition of Ceramics: a Comprehensive Experimental, Analytical and Computational Study of Material Behavior, Fabrication Process and Equipment Design, Drexel University, 2002, https://doi.org/10.17918/etd-22.
[32] K.-S. Jaw, C.-K. Hsu, J.-S. Lee, The thermal decomposition behaviors of stearic acid, paraffin wax and polyvinyl butyral, Thermochim. Acta (2001) 367–368, https://doi.org/10.1016/S0040-6031(00)00680-8, 165–168.
[33] T.R. Hull, D. Price, Y. Liu, C.L. Wills, J. Brady, An investigation into the decomposition and burning behaviour of Ethylene-vinyl acetate copolymer nanocomposite materials, Polym. Degrad. Stabil. 82 (2003) 365–371, https://doi.org/10.1016/S0141-3910(03)00214-3.
[34] B.-Å. Sultan, E. Sörvik, Thermal degradation of EVA and EBA—a comparison. I. Volatile decomposition products, J. Appl. Polym. Sci. 43 (1991) 1737–1745, https://doi.org/10.1002/app.1991.070430917.
[35] A.A.M. Oliveira, M. Kaviany, K.E. Hrdina, J.W. Halloran, Mass diffusion-controlled bubbling and optimum schedule of thermal degradation of polymeric binders in molded powders, Int. J. Heat Mass Tran. 42 (1999) 3307–3329, https://doi.org/10.1016/S0017-9310(98)90363-5.
[36] M. Trunec, J. Cihlář, Thermal debinding of injection moulded ceramics, J. Eur. Ceram. Soc. 17 (1997) 203–209, https://doi.org/10.1016/S0955-2219(96)00108-2.
[37] L. Gorjan, A. Dakskobler, T. kosmač, Partial wick-debinding of low-pressure powder injection-moulded ceramic parts, J. Eur. Ceram. Soc. 30 (2010) 3013–3021, https://doi.org/10.1016/j.jeurceramsoc.2010.07.011.